

Perturb Initial Features: Generalization of Neural Networks Under Sparse Features for Semi-supervised Node Classification

Yoonhyuk Choi

Seoul National University
Seoul, Republic of Korea
yoonhyuk95@snu.ac.kr

Taewook Ko

Seoul National University
Seoul, Republic of Korea
taewook.ko@snu.ac.kr

Jiho Choi

Seoul National University
Seoul, Republic of Korea
jihochoi@snu.ac.kr

Chong-Kwon Kim

Korea Institute of Energy Technology
Naju, Republic of Korea
ckim@kentech.ac.kr

ABSTRACT

Graph neural networks (GNNs) are commonly used in semi-supervised settings. Previous research has primarily focused on finding appropriate graph filters (e.g., aggregation methods) to improve message-passing schemes. While these methods are effective, they can still suffer from the sparsity of training nodes in case their features have few non-zero elements. This can lead to overfitting in certain dimensions in the first projection matrix, as training samples may not learn the entire dimensions of graph filters (hyperplanes). To address this issue, we propose a novel data augmentation strategy. Specifically, we create additional space for training by flipping both the initial features and the hyperplane, which removes zero elements and reduces the variance of prediction with improved robustness. To the best of our knowledge, this is the first attempt to mitigate the overfitting of GNNs caused by the initial features. Extensive experiments on real-world datasets demonstrate that our proposed technique increases node classification accuracy by up to 46.5% compared to the baseline method.

CCS CONCEPTS

• Computing methodologies → Machine learning.

KEYWORDS

Graph Neural Networks, Graph Representation Learning, Node Features, Generalization of Parameters

ACM Reference Format:

Yoonhyuk Choi, Jiho Choi, Taewook Ko, and Chong-Kwon Kim. 2023. Perturb Initial Features: Generalization of Neural Networks Under Sparse Features for Semi-supervised Node Classification. In *Proceedings of the 31st ACM International Conference on Information and Knowledge Management (CIKM '23)*, October 21–25, 2023, Birmingham, UK. ACM, New York, NY, USA, 11 pages. <https://doi.org/10.1145/>

Permission to make digital or hard copies of all or part of this work for personal or classroom use is granted without fee provided that copies are not made or distributed for profit or commercial advantage and that copies bear this notice and the full citation on the first page. Copyrights for components of this work owned by others than ACM must be honored. Abstracting with credit is permitted. To copy otherwise, or republish, to post on servers or to redistribute to lists, requires prior specific permission and/or a fee. Request permissions from permissions@acm.org.
CIKM '23, October 21–25, 2023, Birmingham, UK.

© 2023 Association for Computing Machinery.
ACM ISBN 978-1-4503-9236-5/22/10...\$15.00
<https://doi.org/10.1145/>

1 INTRODUCTION

Graph neural networks (GNNs) have achieved remarkable improvements in various fields with the influx of graphical data. By concurrently integrating node features and network structures, GNNs have demonstrated powerful capabilities in node and graph classification tasks, as demonstrated in recent studies such as [10, 15, 21, 37]. Message-passing, which aggregates features from neighboring nodes through recursive updates, is known as a crucial component of GNNs [13].

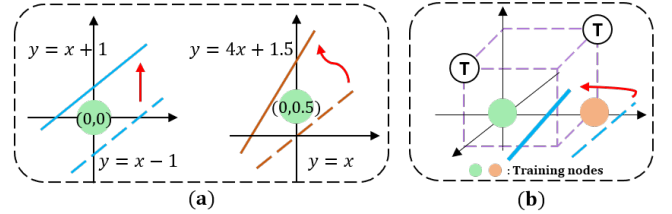


Figure 1: The dotted line is the original line, and the solid one is derived after the update (back-propagation). (a) Gradient updates depend on whether the input data is zero or not. (b) The parameter is optimized for specific dimensions (y -axis), which may fail to classify the test nodes (T)

Recently, many studies have focused on improving aggregation schemes for dealing with heterophilous (disassortative) edges. GNNs generally benefit from message-passing in homophilic graphs [30], where most connected nodes are likely to share the same label. Some algorithms address this by assigning different weights to edges before aggregation [1, 19, 37, 45] or eliminating disassortative edges [29, 46]. Others use distant nodes with high similarity [17, 23, 31] and adopt node-specific propagation with trainable boundaries [41]. We fully understand that the proper selection of aggregation schemes is essential. Nonetheless, we raise another question: *are there other aspects beyond aggregation schemes?*

Contrary to previous methods, we focus on the training of learnable matrices (hyperplanes). Our investigation stems from the observation that when initial features have few non-zero elements (e.g. bag-of-words), a shortage of training samples (in semi-supervised settings) can lead to overfitting of certain dimensions in the first

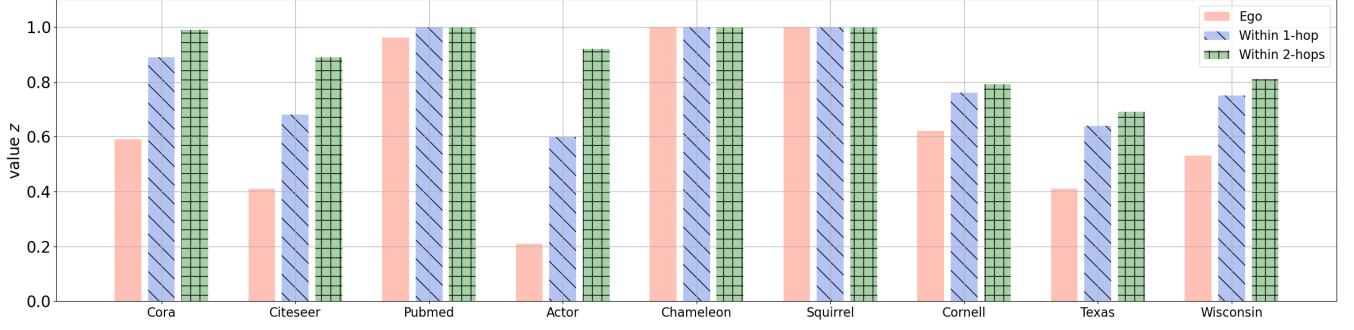


Figure 2: Initial feature distribution of each graph dataset. The definition of value z is described in Equation 4

layer parameters. This can negatively impact the quality of predictions for test nodes with untrained dimensional features.

In Figure 1a, we take two examples that use 2-dimensional input data X (green node) and a plane W (dotted line) to observe the changes in gradients. We apologize for using notations in the introduction to define the problem more intuitively. Let us assume the true label y of both nodes as -1. Then, we can define a loss function \mathcal{L} to update W as below:

$$\hat{y} = W^T X = \sum_{i=1}^2 W_i X_i + b, \quad (1)$$

$$\mathcal{L} = \frac{1}{2} (y - \hat{y})^2, \quad \nabla_W \mathcal{L} = -\eta (y - \hat{y}) X,$$

where $\nabla_W \mathcal{L}$ calculates the partial derivative of a plane. For brevity, we assume the learning ratio η as 1. Since $y = -1$, W can be updated as follow:

$$\begin{pmatrix} W'_1 \\ W'_2 \end{pmatrix} = \begin{pmatrix} W_1 + (-1 - \hat{y})X_1 \\ W_2 + (-1 - \hat{y})X_2 \end{pmatrix}, \quad (2)$$

and also the bias term is updated to $b' = b - (-1 - \hat{y})$.

Back into Figure 1a (left), let us assume the initial line is $y = x - 1$. Since the value of the input feature is $X = (0, 0)$, a plane W is not updated. Instead, the bias becomes $b' = 1 + (-1 - 1) = -1$ which predicts its label as -1 correctly. Likewise, in Figure 1a (right), let us define a line and initial features as $y = x$ and $(0, 0.5)$, respectively. Then, the weights are updated to be:

$$\begin{pmatrix} W'_1 \\ W'_2 \end{pmatrix} = \begin{pmatrix} -1 + (-1 - 0.5) * 0 \\ 1 + (-1 - 0.5) * 0.5 \end{pmatrix} = \begin{pmatrix} -1 \\ 0.25 \end{pmatrix}, \quad (3)$$

and the bias becomes $b' = 0 + (-1 - 0.5) = -1.5$. We can also see that the plane $y = 4x + 1.5$ well classifies the input node $(0, 0.5)$ as negative. Even though both are trained to make accurate predictions, the following examples address the issues associated with zero elements in high-dimensional spaces. In Figure 1b, we consider a scenario where the training samples (colored) are composed of zeros, except for the y -axis. We can infer that only a specific dimension (y -axis) of the plane will be updated, while other dimensions (x and z -axis) remain randomly initialized. This can lead to difficulties in classifying test nodes (T), which can be more problematic if the majority of elements in a high-dimensional space are 0.

To better optimize the first layer matrix that processes initial features, our focus was on the removal of zero elements. Initially, we explored a data augmentation technique such as dimensional

shifting, commonly used in computer vision [34]. However, we found that this approach was not suitable for GNNs with bag-of-words features as it could disrupt the semantic information. Unlike convolutional neural networks, which emphasize local invariance [47], GNNs employ multi-layer perceptrons (MLPs) that are not translation invariant. We also considered the option of adding noise to the inputs [49], but this would entail additional decoding, precise hyper-parameter selection, and normalization challenges [4].

In this paper, we have devised a solution that involves flipping the initial features and parameters simultaneously. This can preserve the volume of gradients and reduce the variance of predictions, which is based on previous techniques such as shifting parameters [20] and rotating neural networks [26]. We also focused on a dual-path network [8] that allows for operation in both the original and flipped spaces. Our method addresses the zero gradient problem caused by input data and promotes accurate semantic learning of each dimension [27]. The flipping mechanism is orthogonal to GNNs and has been applied to five representative methods (MLP, GCN [21], GAT [37], GIN [42], and APPNP [22]). We compared the performance of these flipping variants (Flip-MLP, Flip-GCN, Flip-GAT, Flip-GIN, and Flip-APPNP) with the original methods and observed a relative gain of 16.5%, 24.2%, 17.8%, 13.7 %, and 19.0 % respectively. Further, we confirmed that our approach surpasses all existing state-of-the-art methods in the seven datasets with bag-of-word features. The contributions can be summarized as follows:

- We demonstrate that GNNs are highly sensitive to bag-of-words features and their performance can be significantly improved through flip-based augmentation.
- To secure shift invariance, we propose a flipping mechanism that perturbs both the initial features and the hyperplane. Unlike previous methods that focus on aggregation schemes, our approach examines back-propagation and provides precise component-wise guidance for the first hyperplane.
- The proposed flipping mechanism is orthogonal to the message-passing network, where we develop five flipping variants of GNNs. The extensive experiments on seven real-world benchmark graphs reveal that our flipping variants outperform all existing state-of-the-art baselines significantly.

2 PRELIMINARIES

This section begins with the commonly used notations in Graph Neural Networks (GNNs), which will be utilized throughout this paper. Next, we conduct an empirical analysis to illustrate an overview of the feature distribution in benchmark datasets. Finally, we introduce the mechanism of GNN from the perspectives of feature projection and message-passing.

2.1 Notations

Let $\mathcal{G} = (\mathcal{V}, \mathcal{E})$ be an undirected graph with $|\mathcal{V}| = n$ nodes and $|\mathcal{E}| = m$ edges. The graph connectivity is represented by the adjacency matrix $A \in \{0, 1\}^{n \times n}$. Each node in the graph has properties represented by the feature matrix $X \in \mathbb{R}^{n \times F}$, where F is the number of input dimensions for the initial features. The labels of each node are represented by $Y \in \mathbb{R}^{n \times C}$, where C is the number of classes. The goal of this work is to solve a node classification task in a semi-supervised setting where only a subset of labeled nodes $\mathcal{V}_L \subset \mathcal{V}$ is available for training. Our focus is on how to better utilize the given features to predict the labels of unlabeled nodes $\mathcal{V}_U = \mathcal{V} - \mathcal{V}_L$.

2.2 Empirical Analysis

Given the node set S and their initial features $X \in \mathbb{R}^F$, the ratio of non-zero feature dimensions of S can be defined as below:

$$z = \frac{\sum_{o=1}^{|j|} (1 - \delta_{j_o,0})}{\dim(x)}, \quad j = \sum_{v \in S} X_v. \quad (4)$$

Firstly, we can retrieve $j \in \mathbb{R}^F$ by adding the feature vectors of subset node X_v . The number of non-zero elements in vector j can be defined through the Kronecker delta function δ , where $\delta_{j_o,0} = 1$ if the o -th element in j is 0. Finally, we can retrieve z by dividing the numerator into the feature vector dimension $\dim(x) = F$.

In Figure 2, we display the z by varying the range of node set S from ego to their 2-hop neighboring nodes. As seen, z increases with the range due to the availability of more features during training. Additionally, the scale of z varies significantly for each graph, dependent on the type of input (please refer to the dataset description in § 4.1). In essence, the lower the value of z , the greater the performance improvement obtained from flipping. To further examine this phenomenon, we provide a theoretical explanation in terms of gradient update and variance reduction.

2.3 Graph Neural Network

Recently, spatial GNNs have achieved prominent performance while reducing the computational cost of Laplacian decomposition. Their basic form is given by:

$$H^{(l+1)} = \sigma(\bar{H}^{(l+1)}), \quad \bar{H}^{(l+1)} = AH^{(l)}W^{(l)} \quad (l \geq 1). \quad (5)$$

A stands for a matrix that is used for message-passing. $H^{(1)} = X$ is an initial feature of nodes and $\bar{H}^{(l)}$ is their hidden representation of l -th layer. $H^{(l)}$ can be retrieved through an activation function σ (e.g., ReLU). GNNs obtain the final prediction $\hat{H}^{(L)}$ by applying softmax on it. Here, $W^{(l)}$ is the trainable weight matrices shared across all nodes. They are updated through negative log-likelihood loss (\mathcal{L}_{nll}) between the predicted \hat{Y} and true labels Y as below:

$$\mathcal{L}_{GNN} = \mathcal{L}_{nll}(\hat{Y}, Y), \quad \hat{Y} = \text{softmax}(\hat{H}^{(L)}). \quad (6)$$

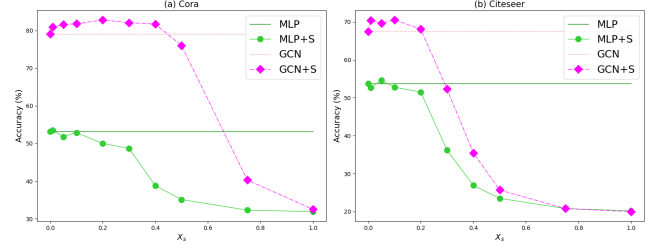


Figure 3: Node classification accuracy when shifting the input features by X_s . Symbol (+S) means shifting is applied on a base model, MLP and GCN [21]

Generally, GNNs focus on improving aggregation schemes to determine an appropriate message-passing scheme [1, 6, 22, 37]. For instance, GCN [21] utilizes a normalized Laplacian matrix, GAT [37] creates an aggregation matrix by calculating the attention score between nodes, and APPNP [22] combines personalized PageRank to enhance the propagation scheme. However, the updates of the first hyperplane based on the input features have not been addressed so far, and we will introduce them in the next section.

3 METHODOLOGY

3.1 Motivation

We first explain the limitation of the generic GNNs. It is undeniable that appropriate aggregation schemes are essential for securing performance. However, as explained below, an aggregation scheme itself cannot solve the improper learning rooted in the sparseness of the initial features. To be more specific, we analyze the update of weight matrices $W^{(l)}$ below:

$$\nabla_{W^{(l)}} J = (AH^{(l)})^T \nabla_{\bar{H}^{(l+1)}} J, \quad l = 1, \dots, L. \quad (7)$$

The $J = \mathcal{L}_{GNN}$ is a full-batch loss defined in Equation 6. Intuitively, the lower value of A can obstruct the gradient flow between dissimilar nodes. Nonetheless, there arises a problem when updating the parameters of initial layer $W^{(1)}$:

$$\begin{aligned} \nabla_{W^{(1)}} J &= (AH^{(1)})^T \nabla_{\bar{H}^{(2)}} J \\ &= (AX)^T \nabla_{\bar{H}^{(2)}} J. \end{aligned} \quad (8)$$

Simply, the gradient of $W^{(1)}$ is derived by differentiating J with respect to $\bar{H}^{(2)}$, and the value of AX determines the scale of a gradient. Here, the gradients become zero for certain dimensions with zero inputs ($\forall_i \in F : X_i = 0 \Rightarrow \nabla_{\bar{H}^{(2)}} J = 0$). Thus, the update of $W^{(1)}$ is independent of the adjacency matrix, which only relies on the sparseness of the input features. Since few training samples are available under semi-supervised settings, we focus on how to remove zero elements in X and guide $W^{(1)}$ to learn the precise meaning of each dimension.

Shifting input features only. To remove the zero elements of initial features X , a simple remedy is shifting, which is commonly used in computer vision. To implement this, a small valued vector X_s can be added to X as below:

$$X' = X + X_s. \quad (9)$$

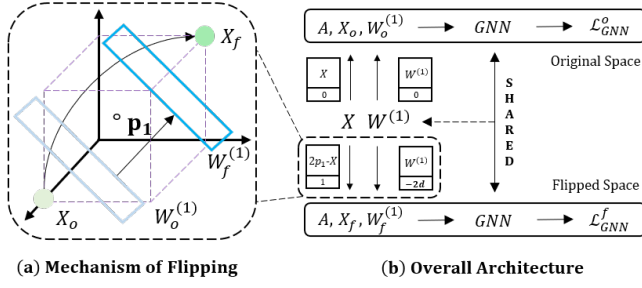


Figure 4: We describe the (a) mechanism of flipping and the (b) overall architecture of Flip-GNN. The parameter of GNN (W) is shared and updated iteratively on both spaces

In Figure 3, we measure the node classification accuracy of MLP and GCN with two layers. Further, we take MLP+S and GCN+S, which take shifted features X' as inputs. Remarkably, the accuracy of shifted methods decreases as X_s increases. This is because Multi-Layer Perceptron (MLP) is not shift-invariant, where large X_s can lead to decreased robustness [35]. Moreover, shifting changes the magnitude of an input, which is crucial for normalizing neural networks. Thus, we suggest moving the features and the first hyperplane concurrently which will be discussed below.

3.2 Flipped Graph Neural Networks

We present a scheme that simultaneously flips both feature vectors and the hyperplane. If the original feature vector has elements in the range $[0, 1]$, then its symmetric transposition through $p_1 = (0.5, \dots, 0.5)$ will also be in this range (as seen in the hypercube in Figure 4a), with the feature vector $X_o = (1, 0, 0)$ transposing to $X_f = (0, 1, 1)$. This transposition is also applied to the hyperplane $W_o^{(1)}$. The right side of the figure shows the original and flipped spaces in the upper and lower panels, respectively. Our method utilizes a shared parameter on two spaces, while the initial features X and the first hyperplane $W^{(1)}$ are varied in each iteration. Here, we separate $W^{(1)}$ into two parts, $W_o^{(1)}$ and $W_f^{(1)}$, where the subscripts o and f denote the original and flipped spaces, respectively. Again, the symbol ∇ represents the partial derivative of the loss function.

Remark. Instead of flipping, shifting is also applicable. But we have observed slightly better performance when the dimensions activated by the input do not overlap in each space. For simplicity, we implement plane GCN [21] as the convolution layer and the details of our approach will be discussed below.

Original space. In Figure 4b, the upper panel illustrates the plane GCN. It takes X_o and $W_o^{(1)}$ as inputs, which are the zero-padded version of the initial feature matrix X and a first hyperplane $W^{(1)}$ as below:

$$X_o = \begin{pmatrix} X \\ 0 \end{pmatrix}, \quad W_o^{(1)} = \begin{pmatrix} W^{(1)} \\ 0 \end{pmatrix}. \quad (10)$$

Though the last dimension is only utilized in the flipped space, zero-padding is required to ensure dimensional consistency (Fig. 5, left) as $W^{(1)}$ is shared between the two spaces. Now, we can

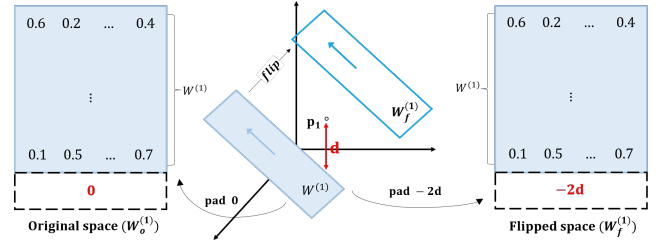


Figure 5: The variation of first hyperplanes. For $W_o^{(1)}$, we pad 0 to the last dimension of $W^{(1)}$ (left). For $W_f^{(1)}$, we measure distance d from $W^{(1)}$ to p_1 and pad $-2d$ to $W^{(1)}$ (right)

compute the loss $J_o = \mathcal{L}_{GNN}(Y, \hat{Y}_o)$ using Eq. 5 and 6 to update the parameter W .

Flipped space. We first define a symbol $p_1 = (0.5, \dots, 0.5) \in \mathcal{R}^F$, which acts as the point used for flipping. While many points could be used as p_1 (e.g., the mean of all nodes), we take the central point of F -dimensional hypercube $(1, \dots, 1) \in \mathcal{R}^F$, where most graph datasets adopt bag-of-words features. The flipped feature X_f transposes X through p_1 and pads 1 as below:

$$X_f = \begin{pmatrix} X' \\ 1 \end{pmatrix}, \quad \text{where } X' = 2p_1 - X. \quad (11)$$

We should also flip the first hyperplane $W^{(1)}$ as described in Figure 5 (right). For this, we calculate a distance vector $d \in \mathcal{R}^F$ between the original hyperplane $W^{(1)}$ and p_1 as:

$$W_f^{(1)} = \begin{pmatrix} W^{(1)} \\ -2d \end{pmatrix}, \quad \text{where } d = \sum_{j=0}^{F-1} (p_1 \otimes W^{(1)})[j]. \quad (12)$$

A symbol \otimes is an element-wise product. Referring to Figure 5 (right), $W_f^{(1)}$ is retrieved by padding $-2d$ to the last element, which makes the output of two spaces origin symmetric $X_o W_o^{(1)} = -X_f W_f^{(1)}$ (this is why we flip the hyperplane concurrently, which can preserve the pair-wise distance of hidden representations). Thus, after the first convolution layer, we should multiply the negative constant to the output $A X_f W_f^{(1)}$ before applying activation function σ as,

$$H_f^{(2)} = \sigma(-A X_f W_f^{(1)}). \quad (13)$$

Through Eq. 13, the equality holds $H_f^{(l)} = H_o^{(l)}$ ($l \geq 2$). Thus, the following layer in a flipped space is identical to the original ones as below:

$$H_f^{(l+1)} = \sigma(\bar{H}_f^{(l+1)}), \quad \bar{H}_f^{(l+1)} = A H_f^{(l)} W^{(l)} \quad (l \geq 2). \quad (14)$$

Finally, the loss \mathcal{L}_{GNN}^f is given by:

$$\mathcal{L}_{GNN}^f = \mathcal{L}_{nll}(Y, \hat{Y}_f), \quad \text{where } \hat{Y}_f = \text{softmax}(\bar{H}_f^{(L)}). \quad (15)$$

Using Eq. 15, $W^{(1)}$ can be updated in a flipped space. We describe the overall mechanism of our method in Alg. 1.

Algorithm 1 The overall mechanism of Flip-GCN

Input: Adjacency matrix A , node features X , parameters θ_G , epoch K , best valid and test acc. $\gamma' = \delta' = 0$, learning rate η

Output: Best test accuracy δ'

```

1: for number of training epoch  $K$  do
2:   # GCN in original space
3:   for training samples do
4:     Given  $X_o$  and  $W_o^{(1)}$ , retrieve the  $\mathcal{L}_{GNN}^o$  (Eq. 6)
5:     Update  $\theta_G^{k+1} = \theta_G^k - \eta \frac{\partial \mathcal{L}_{GNN}^o}{\partial \theta_G^k}$ 
6:   end for
7:   Compute the validation  $\gamma$  and test score  $\delta$ 
8:   if  $\gamma > \gamma'$  then
9:      $\gamma' = \gamma, \delta' = \delta$ 
10:  # GCN in flipped space
11:  for training samples do
12:    Get flipped features  $X_f$  using Eq. 11
13:    Get flipped hyperplane  $W_f^{(1)}$  using Eq. 12
14:    Compute  $\mathcal{L}_{GNN}^f$  through Eq. 15
15:    Update  $\theta_G^{k+2} = \theta_G^{k+1} - \eta \frac{\partial \mathcal{L}_{GNN}^f}{\partial \theta_G^{k+1}}$ 
16:  end for
17:  Compute the validation  $\gamma$  and test score  $\delta$ 
18:  if  $\gamma > \gamma'$  then
19:     $\gamma' = \gamma, \delta' = \delta$ 
20: end for
    
```

3.3 Optimization

We define two loss functions in Eq. 6 and 15. Before gradient analyses, please recall that the equation below holds

$$H_o^{(2)} = \sigma(AX_o W_o^{(1)}) = H_f^{(2)} = \sigma(-AX_f W_f^{(1)}), \quad (16)$$

which implies that the outputs (or gradients) of two different spaces are equivalent after the first layer as below:

$$\nabla_{W_o^{(l)}} J_o = \nabla_{W_f^{(l)}} J_f \quad (l \geq 2). \quad (17)$$

Similar to J_o , the $J_f = \mathcal{L}_{GNN}^f$ is a full-batch gradient in the flipped space (Eq. 15). We employ ReLU as an activation function. Now, referring to Eq. 8, we define the gradients of the first hyperplane $W^{(1)}$ on both spaces.

In the original space, update $W_o^{(1)}$ as,

$$\nabla_{W_o^{(1)}} J_o = (AX_o)^T \nabla_{\bar{H}_o^{(2)}} J_o, \quad \bar{H}_o^{(2)} = AX_o W_o^{(1)}. \quad (18)$$

In the flipped space, update $W_f^{(1)}$ as,

$$\nabla_{W_f^{(1)}} J_f = -(AX_f)^T \nabla_{\bar{H}_f^{(2)}} J_f, \quad \bar{H}_f^{(2)} = AX_f W_f^{(1)}, \quad (19)$$

where the negative constant is multiplied by the gradient since we flipped the sign of output $AX_f W_f^{(1)}$ in Eq. 13.

Proof of convergence. We show that our optimization guarantees the convergence of $W^{(1)}$. If the activation function ensures

origin symmetry, we can redefine Eq. 18 and 19 as:

$$\begin{aligned} \nabla_{W_o^{(1)}} J_o &= (AX)^T \nabla_{\bar{H}_o^{(2)}} J_o, \\ \nabla_{W_f^{(1)}} J_f &= A(2p_1 - X)^T \nabla_{\bar{H}_f^{(2)}} J_f. \end{aligned} \quad (20)$$

Here, the gradient of each dimension in $W^{(1)}$ is proportional to that of X and $2p_1 - X$, respectively. Also, it gets closer to a local optimum $W_*^{(1)}$ as the iteration T increases $\mathbb{E}[W_T^{(1)} - W_*^{(1)}]^2 \propto \frac{\log T}{T}$ [24] since the two-layer neural networks with a ReLU activation converge to a local minimum. Note that gradient ∇J and parameters $|W_o^{(l)}|, |W_f^{(l)}|$ are all bounded. These properties guarantee the convergence of parameters [5]. Finally, we notice that adjusting the scale of gradients for each dimension can stabilize our model:

$$W_o = W_o - \alpha \nabla_{W_o} J_o, \quad W_f = W_f - \beta \nabla_{W_f} J_f, \quad (21)$$

where the α and β can be derived through a grid search.

3.4 Computational Complexity

To analyze the computational complexity, we divide our model into two parts. The proposed scheme consists of a vanilla GCN [21] and a flipped GCN. The computational cost of vanilla GCN is known to be $O(|\mathcal{E}|P_{GCN})$, where P_{GCN} is the number of learnable weights. More specifically, P_{GCN} can be decomposed [48] into $O(nz(X)F' + F'C)$, where $nz(X)$ is the number of non-zero elements in input X and F' is the dimension after projection. $F'C$ is the parameter of the second convolution layer. Also, $O|\mathcal{E}| \approx O|\mathcal{E}|d_{max}$ and d_{max} is the maximum degree. Similar to the vanilla GCN, the complexity of the flipped GCN can be defined as $O(|\mathcal{E}|P'_{GCN})$. In detail, $P'_{GCN} = O(nz(X_f)F' + F'C)$ where $nz(X_f)$ is the number of non-zero elements in flipped features. Summarizing the above two equations, the complexity of our model is $O(|\mathcal{E}|(P_{GCN} + P'_{GCN}))$, which is proportional to the number of edges ($|\mathcal{E}|$) and the size of learnable matrices ($P_{GCN} + P'_{GCN}$).

3.5 Theoretical Analysis

Data augmentation is closely related to empirical risk minimization, which can be explained through *bias-variance tradeoff* [7]. Here, we prove that flipping acts as an augmentation strategy, generalizing the trainable parameters by reducing the variance of predictions. Firstly, let us assume the plane estimator as $g(X_o) = GNN(X_o)$ that is trained only with original feature X_o , and the augmented network as $\bar{g}(X) = GNN(X)$ that uses both features $X = \{X_o \cup X_f\}$. We can easily see that function g is invariant to flipping since $g(X_o, W_o) = g(X_f, W_f)$ and X_f preserves the pair-wise distance between nodes. As the bias term vanishes under the invariance (concurrent flip of a hyperplane), we focus on the variance of $g(X)$, which can be decomposed by the law of total covariance:

$$\begin{aligned} Cov(g(X)) &= Cov(\mathbb{E}[g(X)]) + \mathbb{E}[Cov(g(X))] \\ &= Cov(\bar{g}(X)) + \mathbb{E}[Cov(g(X))]. \end{aligned} \quad (22)$$

Here, $Cov(\mathbb{E}[g(X)]) = Cov(\bar{g}(X))$ since they share the same marginal distribution. Also, $\mathcal{W}_1(\mathbb{E}[g(X)], \mathbb{E}[\bar{g}(X)])$, which is the difference of their mean equals to the Wasserstein distance (e.g., L_2) between two distributions and independent of the total variance. Based on this observation, we can induce the condition below:

$$Cov(\bar{g}(X)) \leq Cov(g(X)). \quad (23)$$

Table 1: Statistical details of nine benchmark graph datasets

Datasets	Cora	Citeseer	Pubmed	Actor	Chameleon	Squirrel	Cornell	Texas	Wisconsin
# Nodes	2,708	3,327	19,717	7,600	2,277	5,201	183	183	251
# Edges	10,558	9,104	88,648	25,944	33,824	211,872	295	309	499
# Features	1,433	3,703	500	931	2,325	2,089	1,703	1,703	1,703
# Classes	7	6	3	5	5	5	5	5	5
# Training Nodes	140	120	60	100	100	100	25	25	25
# Validation Nodes	500	500	500	3,750	1,088	2,550	79	79	113
# Test Nodes	1,000	1,000	1,000	3,750	1,089	2,551	79	79	113

Finally, we show the losses of two networks follow:

$$\mathcal{L}(\tilde{g}(X)) - \mathcal{L}(g(X)) \in -\mathbb{E}[\text{tr}(\text{Cov}(g(X)))], \quad (24)$$

which means the performance gain of an augmented model depends on the variance reduction compared to a plane method. One can induce a tighter bound of Eq. 22 and 24 using *Loewner order* [7] but we omit them here for the brevity of explanation.

3.6 Analysis of Design Choice

Although plane GNN guarantees convergence to a local optimum, the initial features may lead to overfitting of the first hyperplane. We acknowledge that overfitting is a complex problem, and several schemes, including cross-validation, dropout, and regularization have been proposed to mitigate this issue. However, the problem caused by zero elements (bag-of-words) has received little attention. To address this, we propose perturbing the initial features along with a hyperplane, which preserves the scale of the outputs before and after transposition.

Others may argue that the use of bag-of-words is not solely a problem specific to GNNs, as it is commonly used in many research areas. Nevertheless, the important point is that this issue has a greater impact on GNNs assuming a semi-supervised setting, and our proposed method has demonstrated performance that previous approaches focusing solely on message-passing have not achieved.

4 EXPERIMENTS

We focused our efforts to find answers to the following research questions:

- **RQ1:** Does flipping effectively address the issue of multiple zero values in the initial features?
- **RQ2:** Does flipping ensure convergence?
- **RQ3:** How significant is the difference between the gradients from the original and flipped spaces?
- **RQ4:** How does the performance of flipping change as the number of training samples increases?
- **RQ5:** How much does the hyper-parameter in Eq. 21 affect the overall performance?

4.1 Datasets and Baselines

Details of datasets. Our experiments are conducted on nine datasets whose statistical details are described in Table 1. We also measure

the homophily (h) of each dataset as below:

$$h = \frac{\sum_{(i,j) \in \mathcal{E}} \mathbb{1}(Y_i = Y_j)}{|\mathcal{E}|}. \quad (25)$$

- **Cora, Citeseer, Pubmed** [21] are citation networks. The node features in Cora and Citeseer are binary bag-of-words while Pubmed consists of TF-IDF values.
- **Actor** [36] is an actor co-occurrence graph. The node feature encodes the keywords in the actor’s Wikipedia web pages with binary values.
- **Chameleon, Squirrel** [33] are taken from Wikipedia web pages and have non-zero positive or negative values. The maximum element in each dataset is 46.4 and 70.4, while the minimum values are -0.57 and -0.99, which might not be suitable for our method.
- **Cornell, Texas, Wisconsin**¹ contain web pages from computer science departments of multiple universities. The node features are binary bag-of-words, similar to the citation networks.
- **Another datasets.** In addition to the above datasets, recent work [25] introduces large scale non-homophilous graphs. Here, we notice that about half of them (Penn94, pokec, snap-patents) implicate zero-element issues while others are not. Due to the limited space in the main text, we did not conduct experiments with the respective datasets. However, it is evident that a flip is still necessary for benchmark graphs.

Baselines. To show the efficacy of flipping, we employ several state-of-the-art methods.

- **MLP** [32] adopts a feed-forward neural network without message-passing.
- **GCN** [21] suggests the first-order approximation of Chebyshev polynomials [10] to preserve low frequency signals.
- **Ortho-GCN** [14] maintains the orthogonality of feature transformation matrices through three constraints.
- **GAT** [37] employs node features to assign different weights for each edge without graph structural property.
- **GATv2** [2] improves GAT to generate a more dynamic graph attention that is more expressive.
- **GIN** [42] adopts an injective mapping function to enhance the discriminative power of GCN and ensures isomorphism.
- **APPNP** [22] combines personalized PageRank with GCN to improve accuracy while reducing the computational cost.

¹<http://www.cs.cmu.edu/webkb/>

Table 2: (RQ1) Node classification accuracy (%) on nine benchmark graphs. Bold with (*) indicates the best and the gray-colored cell means the top 3 performances. Methods with † are built upon GCN. We show α, β that achieves the best accuracy (Eq. 21)

Datasets	Cora	Citeseer	Pubmed	Actor	Chameleon	Squirrel	Cornell	Texas	Wisconsin
z (Eq. 4)	0.59	0.41	0.96	0.21	1.0	1.0	0.62	0.41	0.53
Homophily (Eq. 25)	0.81	0.74	0.8	0.22	0.23	0.22	0.11	0.06	0.16
MLP	53.2 \pm 0.5 %	53.7 \pm 1.7 %	69.7 \pm 0.4 %	27.9 \pm 1.1 %	41.2 \pm 1.8 %	26.5 \pm 0.6 %	60.1 \pm 1.2 %	65.8 \pm 5.0 %	73.5 \pm 5.4 %
GCN [†]	79.1 \pm 0.7 %	67.5 \pm 0.3 %	77.8 \pm 0.2 %	20.4 \pm 0.6 %	49.4 \pm 0.7 %	31.8 \pm 0.9 %	39.4 \pm 4.3 %	47.6 \pm 0.7 %	40.5 \pm 1.9 %
Ortho-GCN [†]	80.6 \pm 0.4 %	69.5 \pm 0.3 %	76.9 \pm 0.3 %	21.4 \pm 1.6 %	46.7 \pm 0.5 %	31.3 \pm 0.6 %	45.4 \pm 4.7 %	53.1 \pm 3.9 %	46.6 \pm 5.8 %
GAT	80.1 \pm 0.6 %	68.0 \pm 0.7 %	78.0 \pm 0.4 %	22.5 \pm 0.3 %	46.9 \pm 0.8 %	30.8 \pm 0.9 %	42.1 \pm 3.1 %	49.2 \pm 4.4 %	45.8 \pm 5.3 %
GATv2	79.5 \pm 0.5 %	67.4 \pm 0.6 %	76.2 \pm 0.5 %	22.1 \pm 2.0 %	48.3 \pm 0.4 %	28.9 \pm 1.2 %	38.0 \pm 3.8 %	52.5 \pm 1.7 %	41.7 \pm 5.1 %
GIN	77.3 \pm 0.8 %	66.1 \pm 0.6 %	77.1 \pm 0.7 %	24.6 \pm 0.8 %	49.1 \pm 0.7 %	28.4 \pm 2.2 %	42.9 \pm 4.6 %	53.5 \pm 3.0 %	38.2 \pm 1.5 %
APPNP	81.2 \pm 0.4 %	68.9 \pm 0.3 %	79.0 \pm 0.2 %	21.5 \pm 0.5 %	45.0 \pm 0.5 %	30.3 \pm 0.6 %	49.8 \pm 3.6 %	56.1 \pm 0.2 %	45.7 \pm 1.7 %
GCNII	80.8 \pm 0.7 %	69.0 \pm 1.4 %	78.8 \pm 0.4 %	26.1 \pm 1.2 %	45.1 \pm 0.5 %	28.1 \pm 0.7 %	62.5 \pm 0.5 %	69.3 \pm 2.1 %	63.2 \pm 3.0 %
H ₂ GCN	79.5 \pm 0.6 %	67.4 \pm 0.5 %	78.7 \pm 0.3 %	25.8 \pm 1.2 %	47.3 \pm 0.9 %	31.1 \pm 0.5 %	59.8 \pm 3.7 %	66.3 \pm 4.6 %	61.5 \pm 4.4 %
P-reg [†]	80.0 \pm 0.8 %	69.2 \pm 0.7 %	77.4 \pm 0.4 %	20.9 \pm 0.5 %	49.1 \pm 0.1 %	33.6* \pm 0.4 %	44.9 \pm 3.1 %	58.5 \pm 4.2 %	53.7 \pm 2.6 %
FAGCN	81.0 \pm 0.3 %	68.3 \pm 0.6 %	78.9 \pm 0.4 %	26.7 \pm 0.8 %	46.8 \pm 0.6 %	29.9 \pm 0.5 %	46.5 \pm 1.7 %	53.8 \pm 1.2 %	51.0 \pm 4.1 %
GPR-GNN	82.2 \pm 0.4 %	70.1 \pm 0.8 %	79.3 \pm 0.3 %	25.1 \pm 0.5 %	50.9 \pm 0.8 %	30.4 \pm 0.4 %	53.1 \pm 1.6 %	61.2 \pm 0.9 %	62.4 \pm 1.2 %
ACM-GCN	80.2 \pm 0.8 %	68.3 \pm 1.1 %	78.1 \pm 0.5 %	24.9 \pm 2.0 %	49.5 \pm 0.7 %	31.6 \pm 0.4 %	55.6 \pm 3.3 %	58.9 \pm 2.6 %	61.3 \pm 0.5 %
JacobiConv	81.9 \pm 0.6 %	69.6 \pm 0.8 %	78.5 \pm 0.4 %	25.7 \pm 1.2 %	52.8* \pm 0.9 %	32.0 \pm 0.6 %	55.3 \pm 3.4 %	57.7 \pm 3.6 %	53.4 \pm 1.6 %
GloGNN	82.4 \pm 0.3 %	70.3 \pm 0.5 %	79.3 \pm 0.2 %	26.6 \pm 0.7 %	48.2 \pm 0.3 %	28.8 \pm 0.8 %	56.8 \pm 1.1 %	63.0 \pm 2.9 %	59.5 \pm 1.3 %
Flip-MLP	61.4 \pm 0.7 %	60.3 \pm 0.5 %	74.1 \pm 0.5 %	35.9* \pm 0.5 %	43.5 \pm 1.2 %	28.5 \pm 0.8 %	70.5* \pm 4.1 %	79.2* \pm 3.6 %	80.5* \pm 5.1 %
vs MLP (+ %)	+ 15.4 %	+ 12.1 %	+ 6.3 %	+ 28.7 %	+ 2.3 %	+ 2.1 %	+ 17.3 %	+ 20.4 %	+ 9.5 %
α, β	1, 0.1	1, 1	1, 0.01	0.1, 0.1	1, 1	1, 1	0.1, 0.1	0.1, 0.01	1, 1
Flip-GCN [†]	82.7 \pm 0.5 %	72.4 \pm 0.4 %	79.2 \pm 0.2 %	28.6 \pm 0.3 %	50.4 \pm 0.5 %	32.4 \pm 0.3 %	49.4 \pm 0.6 %	62.2 \pm 1.8 %	52.3 \pm 2.4 %
vs GCN (+ %)	+ 4.6 %	+ 7.3 %	+ 1.8 %	+ 40.2 %	+ 2.0 %	+ 1.9 %	+ 20.4 %	+ 30.7 %	+ 29.1 %
α, β	0.1, 0.01	0.01, 1e ⁻³	1, 0.01	1e ⁻³ , 1e ⁻³	1, 1e ⁻³	1, 0.01	1, 1e ⁻³	1, 1e ⁻³	0.01, 1e ⁻³
Flip-GAT	83.1 \pm 0.6 %	72.8 \pm 0.4 %	78.5 \pm 0.2 %	30.3 \pm 0.8 %	48.3 \pm 0.3 %	31.9 \pm 0.5 %	51.9 \pm 1.4 %	61.0 \pm 1.1 %	54.5 \pm 2.1 %
vs GAT (+ %)	+ 3.7 %	+ 7.1 %	+ 0.6 %	+ 34.7 %	+ 3.0 %	+ 3.6 %	+ 20.2 %	+ 22.0 %	+ 19.0 %
α, β	1, 0.1	0.01, 1e ⁻³	1, 1e ⁻³	0.1, 0.1	1, 0.1	1, 1	0.1, 1e ⁻³	0.1, 1e ⁻³	0.1, 1e ⁻³
Flip-GIN	79.5 \pm 0.8 %	69.3 \pm 0.9 %	78.3 \pm 0.5 %	28.5 \pm 0.5 %	50.0 \pm 0.7 %	28.6 \pm 1.1 %	48.1 \pm 2.3 %	57.3 \pm 1.9 %	53.9 \pm 1.7 %
vs GIN (+ %)	+ 2.8 %	+ 4.8 %	+ 1.6 %	+ 15.9 %	+ 1.8 %	+ 1 %	+ 12.1 %	+ 7.1 %	+ 39.3 %
α, β	1e ⁻³ , 1e ⁻³	0.1, 1e ⁻³	1, 0.1	0.01, 0.01	1, 1e ⁻³	1, 0.1	1, 1e ⁻³	1, 1e ⁻³	0.01, 1e ⁻³
Flip-APPNP	83.3* \pm 0.3 %	72.9* \pm 2.3 %	79.6* \pm 0.4 %	31.5 \pm 0.5 %	45.6 \pm 0.5 %	30.4 \pm 0.4 %	56.8 \pm 1.5 %	62.8 \pm 0.5 %	61.0 \pm 2.8 %
vs APPNP (+ %)	+ 2.6 %	+ 5.8 %	+ 0.7 %	+ 46.5 %	+ 1.3 %	+ 0.1 %	+ 14.1 %	+ 11.9 %	+ 33.5 %
α, β	1, 0.01	0.1, 1e ⁻³	1, 0.01	0.01, 0.01	1, 0.01	0.1, 0.01	1, 0.01	1, 1e ⁻³	0.1, 0.01

- **GCNII** [6] further utilizes the weighted identity mapping function to redeem the deficiency of APPNP.
- **H₂GCN** [48] separates ego from neighbors and applies hop-based aggregation for heterophilic networks.
- **P-reg** [44] improves the traditional graph Laplacian to provide extra information that GNNs might not capture.
- **FAGCN** [1] adaptively controls the propagation of low and high-frequency signals during message passing.
- **GPRGNN** [9] introduces an adaptive PageRank to generalize for both homophilic and heterophilic graphs.
- **ACM-GCN** [28] proposes an adaptive channel mixing to capture the diverse information of homophily and heterophily.
- **JacobiConv** [40] analyzes the expressive power of spectral GNN and suggests a Jacobi basis convolution.
- **GloGNN** [23] generates the node embedding by receiving information from global nodes.

Implementation details. We implemented all methods using *PyTorch Geometric*². In detail, two layers of GNNs are used for all baselines except for APPNP and GCNII. The hidden dimension is set

as 64 and we adopted the ReLU with dropout as an activation function. The log Softmax is applied for classification. A learning ratio of (1e⁻³) and the Adam optimizer with a weight decay (5e⁻⁴) are used for training. We randomly chose 20 nodes per class as training samples except for the WebKB dataset whose size is smaller than the others. Then, the remaining nodes are randomly and equally divided into validation and testing nodes except for the citation networks, where we followed [21]. The test accuracy is measured at each iteration, and we selected one that achieves the best validation score. Our source code is also available at anonymous *github*³.

Details of other flip-based methods. Since the first layer of Flip-MLP, Flip-GIN, and Flip-APPNP is a simple projection matrix, we apply Eq. 11 and 12 followed by a sign flip in Eq. 13. Since Flip-GAT utilizes an attention layer and the output of the first layer in a flipped space is symmetric to the original ones, we should multiply the negative constant to retrieve the identical attention weights. The implementation of these flip-variants can also be found in the provided code above.

²<https://pytorch-geometric.readthedocs.io/en/latest/modules/nn.html>

³<https://anonymous.4open.science/r/Flip-GNN-EAA5>

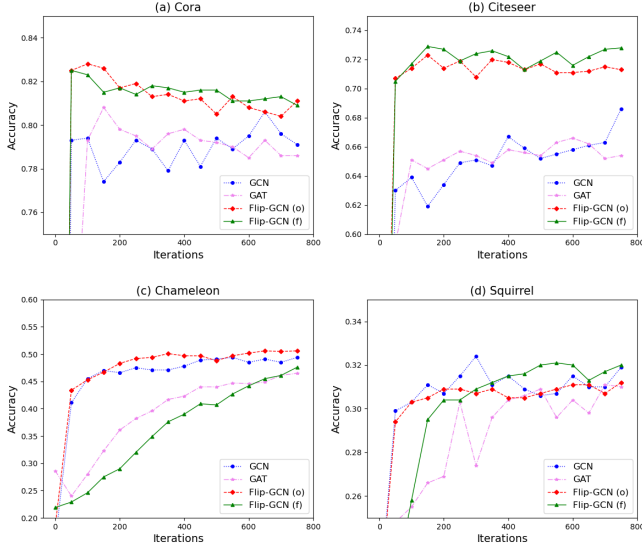


Figure 6: (RQ2) Node classification accuracy (%) of GCN, GAT, and Flip-GCN according to the iteration. The performance of Flip-GCN is measured in the original (o) and flipped (f) space, respectively

4.2 Results and Discussion (RQ1)

In Table 2, we describe the node classification accuracy of all methods. Now, we analyze them from two perspectives below.

Performance gain of flipping is sensitive to the Z-value (Eq. 2) of each dataset. Since flipping is designed to reduce overfitting caused by the sparsity in initial features, we can easily presume that z-value, the non-zero element ratio, is the key factor that determines the performance gains of flipping. Indeed, flipping attains more significant performance gains on low z-valued datasets than on higher ones. For three datasets with higher z (Pubmed, Chameleon, and Squirrel), the advancement of flipping over their vanilla models (e.g., Flip-MLP vs MLP) is relatively small. Nonetheless, five flipping variants outperform the original methods achieving relative improvement of 3 %, 1.9 %, 2.4 %, 1.5 %, and 0.7 % respectively, indicating the effectiveness of flipping even for non-zero initials. On another dataset with low z-values, the flipped methods obtain remarkable advancement over their bases achieving 16.5 %, 24.2 %, 17.8 %, 13.7 %, and 19.0 % on average. Notably, Flip-methods perform best except for Chameleon and Squirrel (with high z and low homophily). This may imply that a slight perturbation to the input features can have a greater impact than aggregation scheme modifications under semi-supervised settings.

The performance is also relevant to the homophily ratio. As stated in Eq. 25, message-passing GNNs utilize the homophily property commonly observed in graphs [25, 43]. Among the three citation graphs, GNNs outperform Multi-Layer Perceptron (MLP) due to the presence of higher homophily ratios. However, in other datasets such as Actor and the three WebKB networks, MLP achieves the highest accuracy among the baselines, indicating that message-passing fails to generalize well in the presence

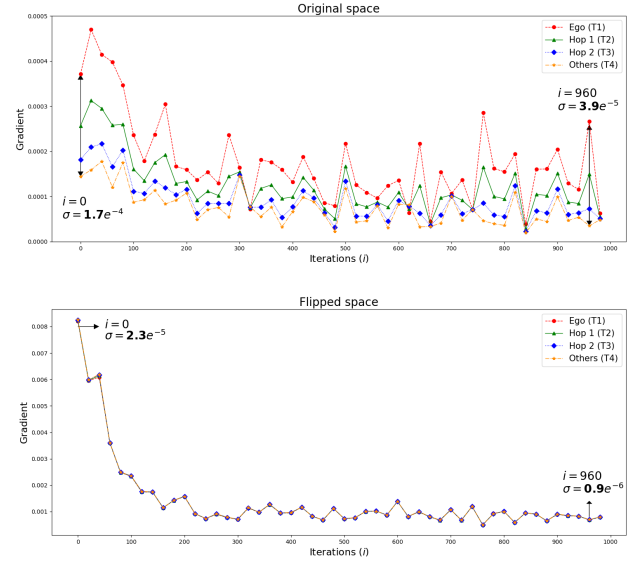


Figure 7: (RQ3) Using the Cora dataset, we plot the magnitude of the first projection matrix gradients and their standard deviation (σ) during training epochs (i)

of high heterophily. The performance gain of Flip-MLP is higher than Flip-GNNs on homophilic graphs, but GNNs benefit more from flipping on heterophilic graphs. While some state-of-the-art methods (GPR-GNN, GloGNN, P-reg, JacobiConv) achieved notable performance, our flipping methods outperform all baselines in seven graph datasets, except for the Chameleon and Squirrel.

4.3 Convergence Analysis (RQ2)

One may argue that flipping could negatively impact the stability of the algorithms due to the operations in two spaces. Figure 6 illustrates the performance of vanilla GCN and GAT compared to Flip-GCN in both spaces as a function of the number of iterations, with results shown for four datasets due to limited space. The performance of GCN (blue), GAT (pink), Flip-GCN (o) in the original space (red), and Flip-GCN (f) in the flipped space (green) are depicted with different colors. The x-axis represents the training epochs, and the y-axis shows the node classification accuracy.

Through this figure, we can see that the flip-GCN achieves higher performance than plain algorithms on both spaces. In the Chameleon graph, please note that flip-GCN (f) surpasses the baselines after 800 epochs. In comparison to GCN and GAT, the flip-based method demonstrates stability and fast convergence, as seen in the Chameleon and Squirrel datasets. This aligns with our analysis, as flipping reduces the variance of predictions, as described in Section 3.5. Though we admit that the performance gain of flip-GCN is dependent on the type of initial features, flip leads to the faster convergence of a model as described in the Chameleon and Squirrel dataset. In conclusion, as a data augmentation strategy, flipping leads to improved performance on datasets with multiple zero elements, while ensuring stable convergence and robustness, which is important in semi-supervised settings.

Table 3: (RQ4) Node classification accuracy (%) w.r.t. the different number of training samples (L/C). The symbol (+F) means that flipping is applied on a base method

Dataset	Cora			Citeseer			Actor			Chameleon			Cornell			Texas		
L/C	20	40	80	20	40	80	20	40	80	20	40	80	5	10	20	5	10	20
z	0.59	0.76	0.91	0.41	0.59	0.78	0.21	0.34	0.5	1	1	1	0.62	0.72	0.84	0.41	0.63	0.78
MLP	53.2	56.9	62.1	53.7	57.3	63.8	27.9	29.0	30.1	41.2	46.3	49.1	60.1	68.8	73.3	65.8	71.4	75.6
MLP+F	61.4	65.5	70.4	60.3	63.1	67.7	35.9	37.4	38.2	43.5	49.9	51.8	70.5	86.4	95.8	79.2	83.3	94.3
GCN	79.1	82.8	83.4	67.5	69.3	71.5	20.4	20.7	21.1	49.4	53.5	55.7	39.4	50.7	53.3	47.6	52.7	54.7
GCN+F	82.7	84.5	85.5	72.4	73.3	75.6	28.6	29.9	30.7	50.4	54.1	55.9	49.4	54.9	72.8	62.2	65.8	78.6

4.4 Analysis of Gradients on Two Spaces (RQ3)

Figure 7 analyzes the gradient of the first projection matrix during the training phase with the Cora dataset. We apply different ranges of neighboring nodes and define four types: T1, T2, T3, and T4. T1 only consists of the features of the central node (Ego). T2 and T3 include the features of 1-hop and 2-hop neighbors, respectively. T4 consists of the remaining features. We prioritize the types from T1 to T4 to avoid overlap and double-counting of features (note that all $T \in \mathcal{R}^F$ are binarized vectors).

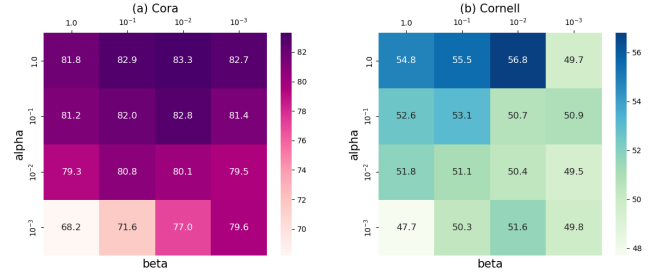
In Figure 7, the average and standard deviation of gradients in two spaces are plotted using different colors. In the original space (upper), the largest gradient is given to features from central nodes, T1 (red) [18]. This is due to the property of GCN, where the gradients generally decrease w.r.t. the hop counts. Also, the features in T4 (orange) have the smallest values, suggesting that they are mostly excluded during training, with only slight updates made by weight regularization. On the other hand, in the flipped space (lower), all types tend to have a similar magnitude with a small deviation (σ) since most dimensions are updated during training.

4.5 Varying the Size of Training Samples (RQ4)

In this experiment, we aim to investigate the impact of labeled sample size on performance. Table 3 displays the z-value of central nodes based on the number of labeled nodes per class (L/C) for six graphs. Here, we adjust the number of training samples to analyze the effect on node classification accuracy.

Firstly, we can see that GCN outperforms MLP on Cora, Citeseer, and Chameleon, while MLP surpasses GCN in other graphs. It shows consistent results even when the L/C increases. Apart from this, we observe that the performance improvement from flipping decreases as the L/C increases. This is because, with more available training nodes, the initial features start to cover most dimensions (high z-value) and the plain models can effectively update the first weight matrix.

In the Chameleon graph, flipping does not have a significant impact on performance as the number of samples increases. This is because the initial features of the dataset are non-zero and have high maximum values, and as the number of labeled nodes increases, the vanilla GCN can perform well as the first hyperplane can generalize without flipping. However, flipping still improves the performance of the base models in the other five graphs significantly, which can contribute to securing robustness and generalization under semi-supervised settings.


Figure 8: (RQ5) Using Flip-APPNP as a base model, we plot node classification accuracy by varying α , β (Eq. 21)

4.6 Hyperparameter Analysis (RQ5)

We analyze how two hyperparameters, α and β in Eq. 21, affect the overall performance of our model. In Figure 8, we illustrate the node classification accuracy of Flip-APPNP by changing α and β through grid search, which adjusts the relative weights of the gradient in two spaces. For evaluation, we employ two types of datasets: Cora (homophilic) and Cornell (heterophilic). Firstly, Flip-APPNP generally outperforms plain APPNP (Cora: 81.2 %, Cornell: 49.8 %) when α is close to 1. Since the original space allows for fast optimization with a small number of elements, the performance decreases in proportion to α . Furthermore, we noticed that assigning small values to β achieves better performance, where the scale of gradients in a flipped space is generally larger than the original ones (please refer to Fig. 7). The corresponding parameters can be found based on the validation score with the highest values.

5 RELATED WORK

Graph Neural Networks. Generally, GNNs can be divided into two categories: spectral-based and spatial-based. Spectral-based GNNs establish a mathematical foundation for graph convolution operations in the spectral domain using the Laplacian matrix [3, 10, 11]. On the other hand, spatial-based GNNs aggregate information from local neighborhoods from a spatial perspective, leading to the development of many aggregation schemes for handling noisy connections [1, 9, 23, 28, 31, 37, 40, 48]. Nonetheless, prior methods only focused on the renovation of message-passing, while sparseness of initial features has not received much attention in literature.

Generalization of neural networks. In the field of neural network generalization, many approaches have been proposed [5, 12, 39]. Several suggested the normalization of deep neural networks [16] while others applied regularization to all adjacent nodes

[44] or integrated label propagation to give further information [38]. More recently, the orthogonal GCN [14] attacks the gradient vanishing problem at the initial few layers of GNNs. RawlsGCN [18] claims the unfairness of gradient update which is biased to nodes with a large degree. Though these methods show notable improvements under the semi-supervised scenario, they fail to solve the problem that is inherently occurred by a characteristic of initial features. In this paper, we solve this problem through a simple yet effective method, flipping.

6 CONCLUSION

Existing GNNs have primarily focused on optimizing the aggregation strategy while neglecting the type of initial features. In this paper, we examine the correlation between zero elements in input vectors and their impact on the first layer of neural networks. We introduce a co-training approach that involves learning the gradient flows in both the original and flipped spaces and adaptively adjusting the parameters. Additionally, we provide a theoretical understanding that flipping reduces prediction variance while maintaining stable convergence. By incorporating flipping into five base methods, we observe an improvement in node classification accuracy, demonstrating that our approach is scalable and effective. In future work, we hope to apply flipping to other variations of GNNs to enhance their performance.

Acknowledgments. The acknowledgment is empty during the review process.

REFERENCES

- [1] Deyu Bo, Xiao Wang, Chuan Shi, and Huawei Shen. 2021. Beyond low-frequency information in graph convolutional networks. *arXiv preprint arXiv:2101.00797* (2021).
- [2] Shaked Brody, Uri Alon, and Eran Yahav. 2021. How attentive are graph attention networks? *arXiv preprint arXiv:2105.14491* (2021).
- [3] Joan Bruna, Wojciech Zaremba, Arthur Szlam, and Yann LeCun. 2013. Spectral networks and locally connected networks on graphs. *arXiv preprint arXiv:1312.6203* (2013).
- [4] Tianle Cai, Shengjie Luo, Keyulu Xu, Di He, Tie-yan Liu, and Liwei Wang. 2021. Graphnorm: A principled approach to accelerating graph neural network training. In *International Conference on Machine Learning*. PMLR, 1204–1215.
- [5] Jianfei Chen, Jun Zhu, and Le Song. 2017. Stochastic training of graph convolutional networks with variance reduction. *arXiv preprint arXiv:1710.10568* (2017).
- [6] Ming Chen, Zhewei Wei, Zengfeng Huang, Bolin Ding, and Yaliang Li. 2020. Simple and deep graph convolutional networks. In *International Conference on Machine Learning*. PMLR, 1725–1735.
- [7] Shuxiao Chen, Edgar Dobriban, and Jane H Lee. 2020. A group-theoretic framework for data augmentation. *The Journal of Machine Learning Research* 21, 1 (2020), 9885–9955.
- [8] Yunpeng Chen, Jianan Li, Huaxin Xiao, Xiaojie Jin, Shuicheng Yan, and Jiashi Feng. 2017. Dual path networks. *Advances in neural information processing systems* 30 (2017).
- [9] Eli Chien, Jianhao Peng, Pan Li, and Olgica Milenkovic. 2020. Adaptive universal generalized pagerank graph neural network. *arXiv preprint arXiv:2006.07988* (2020).
- [10] Michaël Defferrard, Xavier Bresson, and Pierre Vandergheynst. 2016. Convolutional neural networks on graphs with fast localized spectral filtering. *Advances in neural information processing systems* 29 (2016).
- [11] Yushun Dong, Kaize Ding, Brian Jalaian, Shuiwang Ji, and Jundong Li. 2021. Graph neural networks with adaptive frequency response filter. *arXiv preprint arXiv:2104.12840* (2021).
- [12] Jean Feng and Noah Simon. 2017. Sparse-input neural networks for high-dimensional nonparametric regression and classification. *arXiv preprint arXiv:1711.07592* (2017).
- [13] Justin Gilmer, Samuel S Schoenholz, Patrick F Riley, Oriol Vinyals, and George E Dahl. 2017. Neural message passing for quantum chemistry. In *International conference on machine learning*. PMLR, 1263–1272.
- [14] Kai Guo, Kaixiong Zhou, Xia Hu, Yu Li, Yi Chang, and Xin Wang. 2022. Orthogonal graph neural networks. In *Proceedings of the AAAI Conference on Artificial Intelligence*, Vol. 36. 3996–4004.
- [15] Will Hamilton, Zhitaoying, and Jure Leskovec. 2017. Inductive representation learning on large graphs. *Advances in neural information processing systems* 30 (2017).
- [16] Lei Huang, Jie Qin, Yi Zhou, Fan Zhu, Li Liu, and Ling Shao. 2020. Normalization techniques in training dnn: Methodology, analysis and application. *arXiv preprint arXiv:2009.12836* (2020).
- [17] Wei Jin, Tyler Derr, Yiqi Wang, Yao Ma, Zitao Liu, and Jiliang Tang. 2021. Node similarity preserving graph convolutional networks. In *Proceedings of the 14th ACM international conference on web search and data mining*. 148–156.
- [18] Jian Kang, Yan Zhu, Yinglong Xia, Jiebo Luo, and Hanghang Tong. 2022. Rawls-gcn: Towards rawlsian difference principle on graph convolutional network. In *Proceedings of the ACM Web Conference 2022*. 1214–1225.
- [19] Dongkwan Kim and Alice Oh. 2022. How to find your friendly neighborhood: Graph attention design with self-supervision. *arXiv preprint arXiv:2204.04879* (2022).
- [20] Hyungjun Kim, Malte Rasch, Tayfun Gokmen, Takashi Ando, Hiroyuki Miyazoe, Jae-Joon Kim, John Rozen, and Seyoung Kim. 2019. Zero-shifting technique for deep neural network training on resistive cross-point arrays. *arXiv preprint arXiv:1907.10228* (2019).
- [21] Thomas N Kipf and Max Welling. 2016. Semi-supervised classification with graph convolutional networks. *arXiv preprint arXiv:1609.02907* (2016).
- [22] Johannes Klicpera, Aleksandar Bojchevski, and Stephan Günnemann. 2018. Predict then propagate: Graph neural networks meet personalized pagerank. *arXiv preprint arXiv:1810.05997* (2018).
- [23] Xiang Li, Renyu Zhu, Yao Cheng, Caihua Shan, Siqiang Luo, Dongsheng Li, and Weining Qian. 2022. Finding global homophily in graph neural networks when meeting heterophily. In *International Conference on Machine Learning*. PMLR, 13242–13256.
- [24] Yuanzhi Li and Yang Yuan. 2017. Convergence analysis of two-layer neural networks with relu activation. *Advances in neural information processing systems* 30 (2017).
- [25] Derek Lim, Felix Hohne, Xiuyu Li, Sijia Linda Huang, Vaishnavi Gupta, Omkar Bhalerao, and Ser Nam Lim. 2021. Large scale learning on non-homophilous graphs: New benchmarks and strong simple methods. *Advances in Neural Information Processing Systems* 34 (2021), 20887–20902.
- [26] Mingbao Lin, Rongrong Ji, Zihan Xu, Baochang Zhang, Yan Wang, Yongjian Wu, Feiyue Huang, and Chia-Wen Lin. 2020. Rotated binary neural network. *Advances in neural information processing systems* 33 (2020), 7474–7485.
- [27] Hongrui Liu, Binbin Hu, Xiao Wang, Chuan Shi, Zhiqiang Zhang, and Jun Zhou. 2022. Confidence May Cheat: Self-Training on Graph Neural Networks under Distribution Shift. In *Proceedings of the ACM Web Conference 2022*. 1248–1258.
- [28] Sitao Luan, Chenqing Hua, Qincheng Lu, Jiaqi Zhu, Mingde Zhao, Shuyuan Zhang, Xiao-Wen Chang, and Doina Precup. 2022. Revisiting heterophily for graph neural networks. *arXiv preprint arXiv:2210.07606* (2022).
- [29] Dongsheng Luo, Wei Cheng, Wenchao Yu, Bo Zong, Jingchao Ni, Haifeng Chen, and Xiang Zhang. 2021. Learning to drop: Robust graph neural network via topological denoising. In *Proceedings of the 14th ACM International Conference on Web Search and Data Mining*. 779–787.
- [30] Miller McPherson, Lynn Smith-Lovin, and James M Cook. 2001. Birds of a feather: Homophily in social networks. *Annual review of sociology* 27, 1 (2001), 415–444.
- [31] Hongbin Pei, Bingzhe Wei, Kevin Chen-Chuan Chang, Yu Lei, and Bo Yang. 2020. Geom-gcn: Geometric graph convolutional networks. *arXiv preprint arXiv:2002.05287* (2020).
- [32] Marius-Constantin Popescu, Valentina E Balas, Liliana Perescu-Popescu, and Nikos Matorakis. 2009. Multilayer perceptron and neural networks. *WSEAS Transactions on Circuits and Systems* 8, 7 (2009), 579–588.
- [33] Benedek Rozemberczki, Ryan Davies, Rik Sarkar, and Charles Sutton. 2019. Gemsec: Graph embedding with self clustering. In *Proceedings of the 2019 IEEE/ACM international conference on advances in social networks analysis and mining*. 65–72.
- [34] Jia Shijie, Wang Ping, Jia Peiyi, and Hu Siping. 2017. Research on data augmentation for image classification based on convolution neural networks. In *2017 Chinese automation congress (CAC)*. IEEE, 4165–4170.
- [35] Vasu Singla, Songwei Ge, Basri Ronen, and David Jacobs. 2021. Shift Invariance Can Reduce Adversarial Robustness. *Advances in Neural Information Processing Systems* 34 (2021), 1858–1871.
- [36] Jie Tang, Jimeng Sun, Chi Wang, and Zi Yang. 2009. Social influence analysis in large-scale networks. In *Proceedings of the 15th ACM SIGKDD international conference on Knowledge discovery and data mining*. 807–816.
- [37] Petar Velickovic, Guillem Cucurull, Arantxa Casanova, Adriana Romero, Pietro Lio, and Yoshua Bengio. 2017. Graph attention networks. *stat* 1050 (2017), 20.
- [38] Hongwei Wang and Jure Leskovec. 2020. Unifying graph convolutional neural networks and label propagation. *arXiv preprint arXiv:2002.06755* (2020).
- [39] Xiao Wang, Hongrui Liu, Chuan Shi, and Cheng Yang. 2021. Be confident! towards trustworthy graph neural networks via confidence calibration. *Advances in Neural Information Processing Systems* 34 (2021), 23768–23779.

- [40] Xiyuan Wang and Muhan Zhang. 2022. How powerful are spectral graph neural networks. In *International Conference on Machine Learning*. PMLR, 23341–23362.
- [41] Teng Xiao, Zhengyu Chen, Donglin Wang, and Suhang Wang. 2021. Learning how to propagate messages in graph neural networks. In *Proceedings of the 27th ACM SIGKDD Conference on Knowledge Discovery & Data Mining*. 1894–1903.
- [42] Keyulu Xu, Weihua Hu, Jure Leskovec, and Stefanie Jegelka. 2018. How powerful are graph neural networks? *arXiv preprint arXiv:1810.00826* (2018).
- [43] Yujun Yan, Milad Hashemi, Kevin Swersky, Yaoqing Yang, and Danai Koutra. 2021. Two sides of the same coin: Heterophily and oversmoothing in graph convolutional neural networks. *arXiv preprint arXiv:2102.06462* (2021).
- [44] Han Yang, Kaili Ma, and James Cheng. 2021. Rethinking graph regularization for graph neural networks. In *Proceedings of the AAAI Conference on Artificial Intelligence*, Vol. 35. 4573–4581.
- [45] Liang Yang, Fan Wu, Yingkui Wang, Junhua Gu, and Yuanfang Guo. 2019. Masked Graph Convolutional Network.. In *IJCAI*. 4070–4077.
- [46] Zhitao Ying, Dylan Bourgeois, Jiaxuan You, Marinka Zitnik, and Jure Leskovec. 2019. Gnnexplainer: Generating explanations for graph neural networks. *Advances in neural information processing systems* 32 (2019).
- [47] Xin Zhang, Li Liu, Yuxiang Xie, Jie Chen, Lingda Wu, and Matti Pietikainen. 2017. Rotation invariant local binary convolution neural networks. In *Proceedings of the IEEE International Conference on Computer Vision Workshops*. 1210–1219.
- [48] Jiong Zhu, Yujun Yan, Lingxiao Zhao, Mark Heimann, Leman Akoglu, and Danai Koutra. 2020. Beyond homophily in graph neural networks: Current limitations and effective designs. *Advances in Neural Information Processing Systems* 33 (2020), 7793–7804.
- [49] Yanqiao Zhu, Yichen Xu, Feng Yu, Qiang Liu, Shu Wu, and Liang Wang. 2021. Graph contrastive learning with adaptive augmentation. In *Proceedings of the Web Conference 2021*. 2069–2080.